Equinoctial asymmetry of ionospheric vertical plasma drifts and its effect on *F*-region plasma density

Zhipeng Ren,[1] Weixing Wan,[1] Libo Liu,[1] Yiding Chen,[1] and Huijun Le[1]

Received 2 September 2010; revised 25 September 2010; accepted 4 October 2010; published 10 February 2011.

[1] The equinoctial asymmetry of the ionospheric vertical **E** × **B** plasma drift velocity ($V_\perp$) in the equatorial *F* region is investigated based on observations from ROCSAT-1 during 1999 to 2004. It is found that the observed asymmetry exhibits obvious local time dependence with three noticeable features. First, in the Eastern Hemisphere during the interval between 0900 and 1300 LT, $V_\perp$ is obviously higher at the northern spring equinox (March–April) than at the autumn equinox (September–October). Second, there is a pronounced asymmetry for wave number 4 longitudinal structures of $V_\perp$, which exist almost throughout the daytime and even extend into the evening sector at autumn equinox, while they appear mainly at noon and prenoon at spring equinox. Third, around sunset we find an obvious asymmetry of the prereversal enhancement (PRE); the maximum PRE velocity is higher at autumn than at spring equinox in the longitude range from 320° to 150°, and the opposite situation occurs at other longitudes. On the basis of the drift observation mentioned, we also simulate the effect of the $V_\perp$ asymmetry on the ionospheric plasma density by running the Theoretical Ionospheric Model of the Earth, Institute of Geology and Geophysics, Chinese Academy of Sciences (TIME-IGGCAS). It is found that the daytime $V_\perp$ asymmetry can partly explain the equinoctial asymmetry in daytime low-latitude ionospheric plasma density observed by L. Liu et al. (J. Geophys. Res., 115, A09307).

Citation: Ren, Z., W. Wan, L. Liu, Y. Chen, and H. Le (2011), Equinoctial asymmetry of ionospheric vertical plasma drifts and its effect on *F*-region plasma density, *J. Geophys. Res.*, *116*, A02308, doi:10.1029/2010JA016081.

1. Introduction

[2] Although the seasonal variability of the ionosphere has been investigated for several decades [e.g., *Mayr and Mahajan*, 1971; *Rishbeth et al.*, 2000; *L. Liu et al.*, 2007, 2009; *Zhao et al.*, 2007], it still appears on the current list of questions that are not fully resolved [*Rishbeth*, 2004]. Previous works have focused mainly on the differences between summer and winter and between solstice and equinox [e.g., *Ma et al.*, 2003; *Mendillo et al.*, 2005; *Rishbeth et al.*, 2000; *Zhao et al.*, 2007], and most research has assumed that there is no distinction between the two equinoxes. However, some authors have still found that there is obvious equinoctial asymmetry in the ionospheric plasma density [e.g., *Liu et al.*, 2010, and references therein].

[3] The ionospheric equinoctial asymmetry, with the electron density being higher at one equinox than at the other [*Titheridge*, 1973; *Titheridge and Buonsanto*, 1983; *Zhao et al.*, 2007; *Liu et al.*, 2010], is an important ionospheric intra-annual variation. *Titheridge* [1973] studied such asymmetry in the midlatitude ionosphere. *Essex* [1977] detected that the total electron content (TEC) at several stations in the spring equinox (March–April) is usually higher than that in the autumn equinox (September–October). *Bailey et al.* [2000] reported an equinoctial asymmetry in the topside electron density. *Unnikrishnan et al.* [2002] showed that the TEC over Palehua (19°N, 206°E) exhibits opposite equinoctial asymmetries for high and low solar activities. *Wan et al.* [2008] also showed obvious equinoctial asymmetry in longitudinal wave number 4 structures; the wave is stronger in northern autumn months than in spring. Based on the ionospheric electron density profiles and TEC data, *Liu et al.* [2010] investigated the equinoctial asymmetry of the daytime ionosphere during low solar activity. Using long-term observations of incoherent scatter radar (ISRs) chains in the eastern American sector, augmented with the French ISR, *Zhang et al.* [2004, 2005, 2007] studied the local and regional variability of the ionospheric equinoctial asymmetry and their physical mechanisms in detail. A series of other ionospheric parameters, such as electron and ion temperatures, as well as field-parallel and field-perpendicular plasma drifts, also shows obvious equinoctial asymmetry [e.g., *Aruliah et al.*, 1996; *Balan et al.*, 1998; *Kawamura et al.*, 2002; *Zhang et al.*, 2004, 2005, 2007].

[4] The equinoctial asymmetry in the ionosphere may arise mainly from the corresponding asymmetry in the thermosphere, as suggested by *Balan et al.* [1998]. Therefore, the thermospheric equinoctial asymmetry, as well as

[1]Beijing National Observatory of Space Environment, Institute of Geology and Geophysics, Chinese Academy of Sciences, Beijing, China.

0148-0227/11/2010JA016081

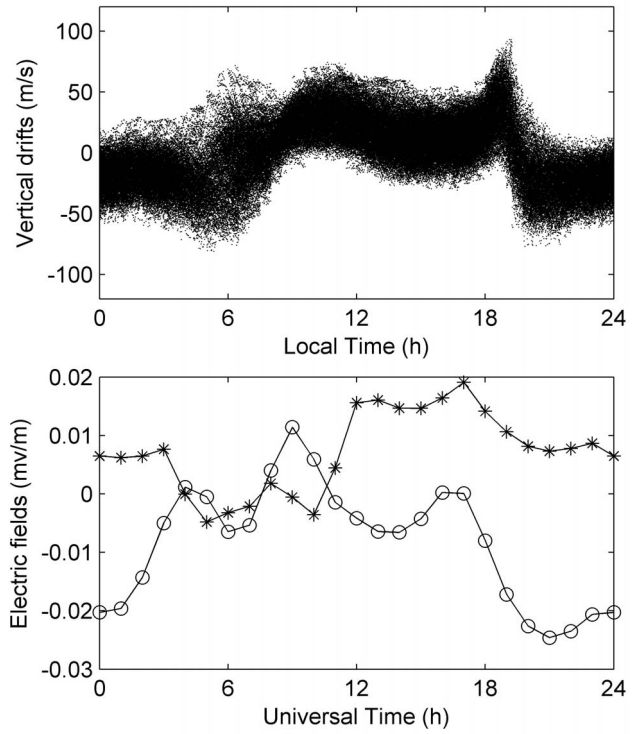

Figure 1. (top) $V_\perp$ pattern observed from ROCSAT-1, which is used in this work. (bottom) Universal time variations of longitudinally average equatorial zonal electric fields for spring equinox (asterisks) and autumn equinox (circles).

the asymmetry in the mesosphere-lower thermosphere (MLT) region, should be very important to reveal the mechanism of ionospheric equinoctial asymmetry and has been studied by several authors [e.g., *Aruliah et al.*, 1996; *Balan et al.*, 1998, 2006]. With the h_mF_2-derived thermospheric winds over Wuhan (30.6°N, 114.4°E), *Liu et al.* [2003] found a prominent equinoctial asymmetry, with the winds being lesser in magnitude in spring equinox than in autumn equinox. Using observations of middle and upper atmosphere (MU) radar, *Balan et al.* [1998] and *Kawamura et al.* [2002] discussed the thermospheric equinoctial asymmetry and its influence on the ionosphere. Recently, *Balan et al.* [2006] studied the equinoctial asymmetry of diurnal mean winds, tides, and waves in both the MLT and the thermospheric *F* regions using MU radar observations in two equinoctial months and suggested that the upper atmospheric regions could be dynamically coupled through mean winds, tides, and waves.

[5] It should be pointed out that the previous works are concerned mainly with high- and mid-latitude thermospheric and ionospheric equinoctial asymmetry. Recently, *Liu et al.* [2010] investigated the behaviors of the daytime ionosphere around equinoxes and found that the equinoctial asymmetry in the ionospheric plasma density during low solar activity is mainly a low-latitude phenomenon. Thus, we need to pay attention to the equinoctial asymmetry in equatorial $V_\perp$, because equatorial *F*-region vertical plasma drifts ($V_\perp$), which are mainly driven by *E*- and *F*-region neutral wind dynamos [e.g., *Heelis*, 2004], play an important role in ionospheric dynamics at equatorial and low latitudes. Perhaps owing to the lack of enough observations, the vertical drift velocity has often been assumed to be in equinoctial symmetry in previous investigations, even though $V_\perp$ equinoctial asymmetry can still be found in some works [e.g., *Kil et al.*, 2009; *Ren et al.*, 2009a, 2010]. In the present work we examine equinoctial asymmetry in the equatorial *F*-region $V_\perp$ based on vertical plasma drift velocity observations by ROCSAT-1. We also simulate the effect of the $V_\perp$ equinoctial asymmetry on the ionospheric plasma density by running the Theoretical Ionospheric Model of the Earth, Institute of Geology and Geophysics, Chinese Academy of Sciences (TIME-IGGCAS).

2. Data and Model

2.1. Measurements and Data Processing

[6] ROCSAT-1 was launched on 27 January 1999 into a circular orbit at an altitude of 600 km with an inclination of 35°. Its orbital period is about 97 min, and consecutive orbits are separated in longitude by about 24.5°. The 24-h local times are covered at latitudes −35° to 35° every 25 days. The Ionospheric Plasma and Electrodynamics Instrument on board ROCSAT-1 operated at 100% duty cycle and made measurements of ion density, temperature, composition, and drift velocity from March 1999 to June 2004. The cross-track plasma drift velocity is measured with the onboard ion drift meter (IDM). The accuracy of the cross-track plasma drift velocity measurements from this IDM depends on the total ion density and the proportion of oxygen ions. The cross-track plasma drift velocity can be determined accurately (error <10%) when the total ion density is higher than 10^3 cm^{-3} and the percentage of oxygen ion exceeds 85%. Because of the near-horizontal magnetic field near the dip equator, the equatorial *F*-region vertical plasma drifts correspond basically to the electrodynamic drift driven by the zonal ionospheric electric fields. Here, to study the equinoctial asymmetry, we use the observations of vertical $\mathbf{E} \times \mathbf{B}$ plasma drifts ($V_\perp$) near the dip equator at equinox (March–April and September–October) from 1999 to 2004.

[7] We only used measurements of $V_\perp$ within 5° of the dip equator, since these measurements have a higher statistical significance. To confine our attention to quiet-time variations, we only use observations during periods of low magnetic activity, marked by $K_p \leq 3$. The top plot in Figure 1 shows all $V_\perp$ data used in this work. We first separate $V_\perp$ data into two 2-month-long seasonal bins: spring equinox (March–April) and autumn equinox (September–October). Then, using a method similar to that of *Ren et al.* [2009a], we remove the effect of solar flux on $V_\perp$ and get local time and longitudinal variations of equinoctial $V_\perp$ in two equinoxes during quiet time for mean solar flux ($F_{10.7}$ = 175). As zonal electric fields' line integrals along the dip equator must be 0 (curl-free condition), we calculate the average zonal electric fields to examine our result. The bottom plot in Figure 1 shows universal time variations of longitudinally average zonal electric fields for spring equinox (asterisks) and autumn equinox (circles). As the equa-

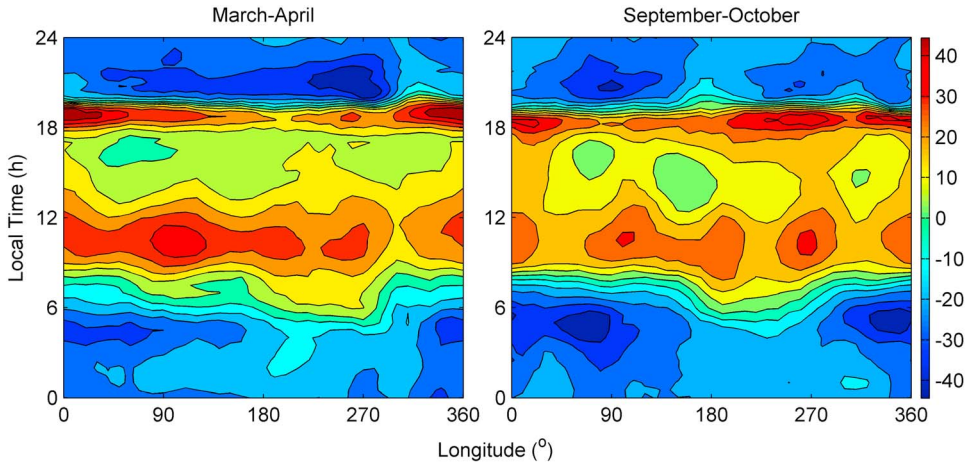

Figure 2. Local time and longitudinal variations of $V_\perp$ in two equinoxes (in unit of m/s).

torial geomagnetic field strength is between 0.19 and 0.30 G at the height of the satellite, the longitudinally averaged zonal electric field (by about 0.02 mV/m) changes the longitudinally averaged $V_\perp$ by about 0.8 m/s. Since we do not know the exact local time and solar-flux-dependent accuracy of the drift measurements, we did not attempt to correct them to satisfy the curl-free condition.

2.2. TIME - IGGCAS and Inputs

[8] *Yue et al.* [2008] developed a mid- and low-latitude theoretical ionospheric model, the TIME-IGGCAS. This model solves the coupled equations of the mass continuity, momentum, and energy of three main ions, O^+, H^+, and He^+, in closed geomagnetic tubes and calculates the densities, temperatures, and field-aligned diffusion velocities of these three main ions as well as electrons. The model also calculates the densities of three minor ions, N_2^+, O_2^+, and NO^+, under the assumption of photochemical equilibrium. In the TIME-IGGCAS model the differences in temperature between the different ions are ignored, and only the temperature of O^+ is calculated. The geomagnetic field in TIME-IGGCAS is an eccentric dipole field. Detailed descriptions of the model including the numerical procedure and the choice of several parameters such as heating rates and collision frequency are given by *Yue et al.* [2008]. Those authors suggest that this model is steady and credible and can reproduce most large-scale features of the ionosphere.

[9] The principal input parameters for the TIME-IGGCAS model, such as neutral winds, neutral temperature, neutral number densities, and vertical $\mathbf{E} \times \mathbf{B}$ plasma drifts, are obtained from observations or from empirical models. In the following simulations the neutral temperature and densities are taken from the NRLMSIS-00 model, and the NO concentration is calculated from an empirical model developed by *Titheridge* [1997]. Neutral winds are determined by the HWM-93 model. F_{107} and *Ap* are needed to represent solar and geomagnetic activities, respectively. In this study the simulations were carried out on a magnetic plane (*np*, *nl*) (*np* = 201, *nl* = 100), where *np* is the number of points along a magnetic field line and *nl* is the number of magnetic field lines, with a time step of 300 s.

3. Results and Discussion

3.1. Equinoctial Asymmetry in Equatorial $V_\perp$

[10] Figure 2 shows the local time and longitudinal variations of $V_\perp$ for spring equinox (left) and autumn equinox (right). As shown in Figure 2, $V_\perp$ values in the two equinoxes show some similar features. We note that the diurnal variations in $V_\perp$ in different longitudinal sectors in both equinoxes are all similar to the diurnal variations in $V_\perp$ observed at Jicamarca in Peru [see *Fejer et al.*, 1991]. As shown in Figure 2, $V_\perp$ values in both equinoxes are upward in the dayside and downward at night. Near 1700–1900 LT there is a sharp increase in upward $V_\perp$, which is known as the PRE. The longitudinal variations in the two equinoxes also show some similar features. The morning drift reversal times in the longitudinal range between 180° and 270°E are obviously earlier than those in the other longitudinal sectors in both equinoxes. There is a wave number 4 longitudinal structure manifest during daytime in both equinoxes, whose upward velocity peaks are located near 10°, 100°, 190°, and 270°E longitude at about 1000 LT. From midnight to sunrise (0000–0600 LT), the downward $V_\perp$ between 150° and 290°E is lower than the other longitudinal sectors in both equinoxes. However, an obvious asymmetry of local time and longitudinal variations in $V_\perp$ between spring equinox and autumn equinox is also found. Here we highlight the equinoctial asymmetry during daytime and the PRE.

[11] We note two features in the daytime equinoctial asymmetry. First, the spring $V_\perp$ in the Eastern Hemisphere between 0900 and 1300 LT is obviously higher than the $V_\perp$ in autumn. To study this detail, the top plot in Figure 3 shows the averaged $V_\perp$ between 1000 and 1200 LT for spring equinox (asterisks) and autumn equinox (circles). As shown in Figure 3 the spring $V_\perp$ in the longitudinal range between 40 and 140°E is nearly 10 m/s higher than the autumn $V_\perp$ in the same range. In autumn the average $V_\perp$ in the Eastern Hemisphere nearly equals that in the Western Hemisphere. However, in spring the average $V_\perp$ in the

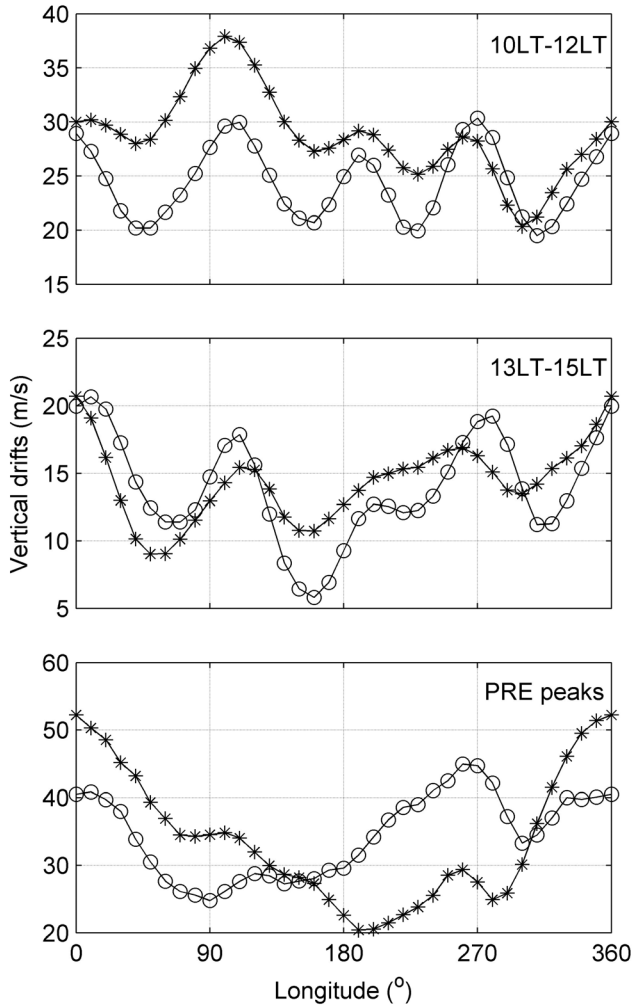

Figure 3. Longitudinal variation of averaged $V_\perp$ at (top) 1000–1200 LT, (middle) 1300–1500 LT, and (bottom) peaks of the prereversal enhancement (PRE) for spring equinox (asterisks) and autumn equinox (circles).

Eastern Hemisphere is obviously higher than that in the Western Hemisphere.

[12] Second, the wave number 4 longitudinal structures of the daytime $V_\perp$ in the two equinoxes are obviously asymmetrical. The wave number 4 longitudinal structure of EEJ and equatorial daytime ionospheric vertical plasma drifts at equinox was recently reported [e.g., *England et al.*, 2006; *Hartman and Heelis*., 2007; *Kil et al.*, 2007; *Fejer et al.*, 2008; *Ren et al.*, 2008, 2009a, 2010]. As shown in Figure 2 this longitudinal structure is obviously stronger in the autumn than in the spring equinox. During autumn equinox this longitudinal structure appears in the morning and generally extends into the evening sector. However, although this longitudinal structure also appears at 0900–1300 LT during spring equinox, it disappears in the afternoon. To demonstrate the detail of this daytime asymmetry, Figure 3 shows the averaged $V_\perp$ between 1000 and 1200 LT (top plot) and between 1300 and 1500 LT (middle plot) for spring equinox (asterisks) and autumn equinox (circles). Although the upward $V_\perp$ at 1000–1200 LT in the Eastern Hemisphere in autumn equinox is higher than that in autumn equinox, the averaged $V_\perp$ in both equinoxes presents a wave number 4 longitudinal structure. At 1300–1500 LT, although the averaged $V_\perp$ in autumn equinox also presents a wave number 4 longitudinal structure, the averaged $V_\perp$ in spring equinox does not show a similar wave number 4 longitudinal structure and presents a three-peak longitudinal structure whose upward velocity peaks are located near 10°, 110°, and 260°E longitude, respectively.

[13] The PRE is an important feature of the equatorial ionospheric vertical plasma drifts. As shown in Figure 2, an obvious equinoctial asymmetry of the PRE is also found. Here we use the maximum velocity (peak) of the PRE as the PRE parameter. The bottom plot in Figure 3 shows the longitudinal variation in the peak velocity of the PRE for spring equinox (asterisks) and autumn equinox (circles). The upward peak velocity of the PRE in autumn equinox is higher than that in spring equinox in the longitudinal range 150° to 320°E, and the upward peak velocity of the PRE in autumn equinox is lower than that in spring equinox in the longitudinal range 320° to 150°E. Note that in the longitudinal range 150° to 320°E the dip equator is mainly in the southern geographical hemisphere, and the dip equator is mainly in the northern geographical hemisphere in the longitudinal range of 320° to 150°E.

[14] As the daytime *E*-region electric conductivity is much higher than that in the *F* region, the daytime ionospheric electric fields and $\mathbf{E} \times \mathbf{B}$ plasma drifts are mainly controlled by an *E*-region dynamo [e.g., *Heelis*, 2004], which is driven primarily by tidal wind that propagates from below [e.g., *Forbes*, 1995]. Thus, the equinoctial asymmetry of the equatorial $V_\perp$ may relate to the asymmetry in the *E*-region tide. Actually, on the basis of ROCSAT-1 observations and model simulations, *Ren et al.* [2009a, 2010] found that the intra-annual variations in equatorial $V_\perp$ of the wave number 4 structure are controlled by the intra-annual variation of the symmetric wind component of the eastward-propagating wave number 3 diurnal (DE3) tide (see also *Oberheide and Forbes* [2008]). On the basis of Sounding of the Atmosphere using Broadband Emission Radiometry (SABER) and Constellation Observing System for Metereology, Ionosphere, & Climate (COSMIC) data, *Pancheva and Mukhtarov* [2010] studied the latitude structure and seasonal variability of nonmigrating DE3 and DE2 tides, in temperature at 110 km and in h_mF_2 during low solar activity, and, also, found that the ionospheric DE3 response is stronger in autumn than in spring. Hence, the equinoctial asymmetry in wave number 4 structure may relate to the asymmetry in the DE3 tide. There are also many other equinoctial asymmetries in *E*-region tides, such as the semiannual oscillation (SAO) in the tropical MLT region. Previous research has suggested that the migrating diurnal tidal amplitude in the tropical MLT region is largest around the two equinoxes (SAO), and the first cycle of the SAO (spring equinox) is stronger than the second cycle (autumn equinox) [e.g., *Dunkerton*, 1982; *Garcia et al.*, 1997; *Mukhtarov et al.*, 2009; *Xu et al.*, 2009]. The stronger-migrating diurnal tide can drive a stronger *E*-region dynamo and a stronger equatorial $V_\perp$. This can explain the stronger daytime equatorial $V_\perp$ near spring equinox in the Eastern Hemisphere. However, we note that the average $V_\perp$ near

spring equinox in the Western Hemisphere is not obviously larger than that near autumn equinox. This phenomenon may imply that it is driven by nonmigrating tides that can drive wave number 1 longitudinal structures, such as westward-propagating wave number 2 diurnal (DW2) and stationary diurnal (D0) tides, westward-propagating wave number 3 and wave number 1 semidiurnal (SW3 and SW1) tides, and stationary planetary wave number 1 (SPW1) tide [*Häusler and Lühr*, 2009]. Thus, more data observations and simulations are needed to study this question.

[15] The PRE is mainly produced by the *F*-layer dynamo, and *Crain et al.* [1993] have proposed that the gradient of the eastward thermospheric neutral wind may be mainly responsible for the PRE at about 1900 LT. Although the longitudinal variations in geomagnetic fields can obviously affect the longitudinal variations in the PRE [e.g. *Ren et al.*, 2009b], we could not explain the equinoctial asymmetry in PRE with the longitudinal variation in geomagnetic fields. Thus, the equinoctial asymmetry in PRE may relate to the equinoctial asymmetry in the eastward thermospheric wind. However, recent simulations of the effect of upward-propagating tidal energy in a global circulation model showed that although several of the major diurnal tidal modes have practically no effect on the PRE for conditions of high solar activity, the PRE is clearly dependent on the magnitude and phase of the semidiurnal tide during periods of low solar activity [*Millward et al.*, 2001]. On the basis of the MU radar observations in two equinoctial months, *Balan et al.* [2006] studied the equinoctial asymmetry of mean winds, tides, and waves in both the MLT and the *F* regions and suggested that the MLT and high-thermosphere regions could be dynamically coupled together through mean winds, tides, and waves. Hence, the equinoctial asymmetry in *E*-region tides may also be able to cause asymmetry in thermospheric wind and drive the equinoctial asymmetry in the PRE. Thus, both the MLT tides and the thermospheric *F*-region wind may play important roles in the generation of the equinox asymmetry in the PRE. We need more work and simulations to study the equinox asymmetry in the PRE.

3.2. Influence of Equinoctial Asymmetry in $V_\perp$ on the Ionosphere

[16] In this section we study the influence of equinoctial asymmetry in $V_\perp$ on the asymmetry of ionospheric plasma density. Based on the equinoctial $V_\perp$ observation mentioned in the above sections, we will simulate their effect on ionospheric equinoctial asymmetry. *Balan et al.* [1998] suggested that the equinoctial asymmetries of the thermospheric wind, temperature and component all can cause the asymmetries in the ionospheric plasma density. Thus, to remove the effect of the asymmetries in thermospheric wind, temperature and component, these two simulations are both performed for spring equinox, but the input $V_\perp$ are respective for spring equinox (case A) and for autumn equinox (case B). The other empirical models, such as MSIS00 and HWN93, are all carried out with Ap = 4 and $F_{10.7}$ = 175.

[17] Figure 4 shows the geomagnetic longitudinal and latitudinal variations in the *F*-region peak electron number density (N_mF_2) at 1400 LT for two simulations. To better compare the simulation results with the observations [see *Liu et al.*, 2010], we shifted the geomagnetic longitude by 71° to the east. This applied shift approximately colocates the 0° longitude in Figure 4 with the geographic 0° meridian. Figure 4a shows the result for case A, and Figure 4b show the result for case B. Although the two results show similar longitudinal and latitudinal variations, there are also some differences in detail. For example, in the East Asia section, the equinoctial asymmetry in case A is obviously stronger than that in case B. To study the details of the differences, we show the difference between case B and case A in Figure 4c. There are also two features in Figure 4c. First, the equinoctial asymmetry in the East Asia section in case A is stronger than that in case B. Second, although the wave near East Asia is weak, there is a wave number 4 longitudinal structure near the equator in the difference. These two features can be explained by the two features of the equinoctial asymmetry in the daytime $V_\perp$.

[18] With the data on ionospheric electron density profiles from Constellation Observing System for Meteorology, Ionosphere, and Climate (COSMIC) mission radio occultation measurements, total electron density (TEC) from TOPEX and Jason-1, and TEC from GPS receivers as well as global ionosonde measurements of the F_2-layer peak electron density (N_mF_2), *Liu et al.* [2010] investigated the equinoctial asymmetry in daytime ionospheric plasma density. Figure 4a of *Liu et al.* [2010] shows a map of the differences in COSMIC N_mF_2 at about 1400 LT between the September and the March equinoxes. Comparing our Figure 4c with Figure 4a of *Liu et al.* [2010], we find that the equinoctial asymmetry in simulations and in observations shows similar amplitude (about -4×10^{-11} to 2×10^{-11} m^{-3}). Although it is not very clear, there is also a wave number 4 longitudinal structure in the observations of *Liu et al.* [2010]. The equinoctial asymmetry near East Asia is strong in both simulations and observations. However, there are also some differences between the simulations and the observations. For example, the asymmetry near North America is stronger in observations, but the asymmetry in simulations is not stronger in this region. In the simulations, the plasma density near the equator in autumn equinox is obviously higher than that in spring equinox. However, the observed plasma density near the equator in autumn equinox is mainly lower than that in spring equinox.

[19] As shown here the observed equinoctial asymmetry in low-latitude plasma density can be partly explained by the asymmetry in daytime $V_\perp$. The difference between simulations and the observations may relate to the equinoctial asymmetry in the thermospheric parameters, such as thermospheric winds, mass density, and components. For example, the work by *H. Liu et al.* [2007] showed that there is an equinoctial asymmetry in thermospheric neutral mass density, and this asymmetry can affect the asymmetry in the ionosphere. The difference between simulations and observations may also relate to the asymmetry in MLT tides. Except for the dynamo mechanism, tide can also drive the acceleration, heating, and compositional mixing in the MLT region and affect the whole coupled ionosphere/thermosphere system. For example, with the interactive thermosphere-ionosphere general circulation model TIGCM model, *Forbes et al.* [1993] simulated the influence of tide on the ionosphere and thermosphere and found that the upward-propagating diurnal and semidiurnal tides obviously affect the zonal mean states of the thermosphere and ionosphere above 100 km. Hence, we need more data observa-

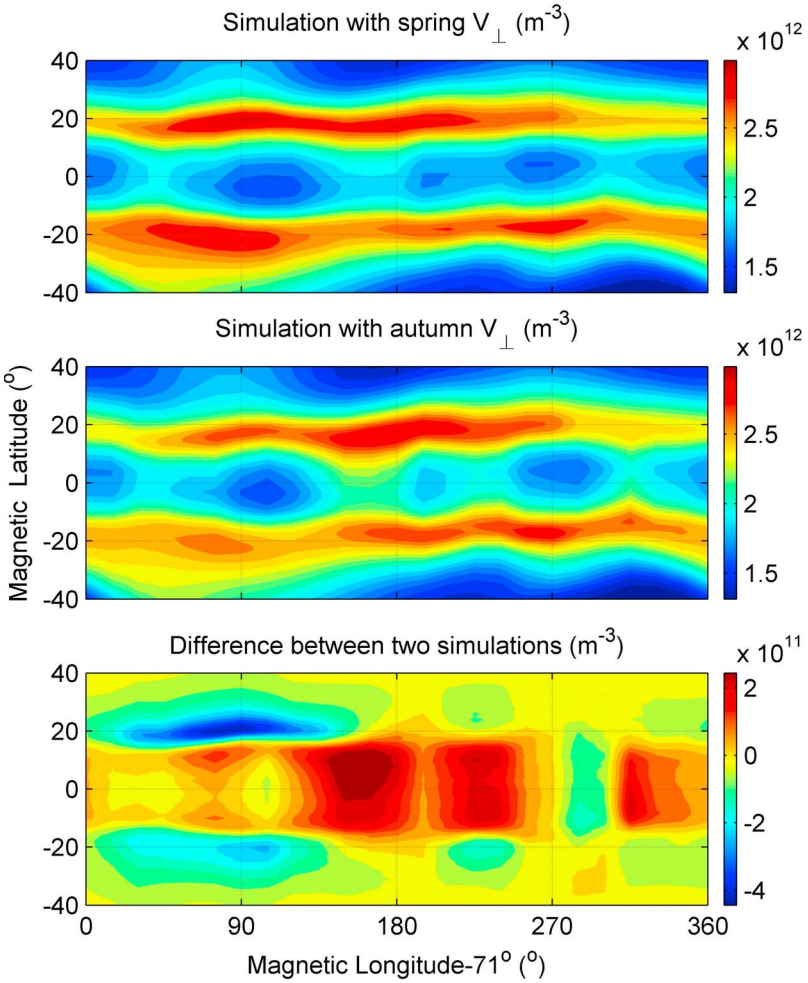

Figure 4. N_mF_2 at 1400 LT from the simulation (top) with spring $V_\perp$ and (middle) with autumn and (bottom) the difference between two N_mF_2 simulations versus geomagnetic latitude and longitude (shifted by 71° to the east).

tions and simulations to understand the physical mechanism of the ionospheric equinoctial asymmetry.

4. Summary and Conclusion

[20] In the present work, vertical plasma drift velocity observations by ROCSAT-1 from 1999 to 2004 have been used to study the equinoctial asymmetry of equatorial F-region vertical $\mathbf{E} \times \mathbf{B}$ plasma drifts ($V_\perp$). It is found that the equinoctial asymmetry depends on the local time. The asymmetry in daytime $V_\perp$ shows two features. First, in the Eastern Hemisphere during the interval between 0900 and 1300 LT, $V_\perp$ is obviously larger at the northern spring equinox (March–April) than at the autumn equinox (September–October). Second, there is a pronounced asymmetry for wave number 4 longitudinal structures of $V_\perp$, which exist during almost all the daytime and even extend to the evening sector at autumn equinox, while they mainly appear at noon and prenoon at spring equinox. The asymmetry in daytime $V_\perp$ may relate to the equinoctial asymmetry in E-region tide. An obvious equinoctial asymmetry of the PRE is also found. The maximum PRE velocity is higher at autumn than at spring equinox in the longitude range from 320° to 150°E, and the opposite case occurs at other longitudes.

[21] On the basis of the drift observation mentioned, we have also simulated the effect of the $V_\perp$ asymmetry on the ionospheric plasma density by running the TIME-IGGCAS model. It is found that the daytime $V_\perp$ asymmetry can partly explain the equinoctial asymmetry in daytime low-latitude ionospheric plasma density observed by *Liu et al.* [2010].

[22] **Acknowledgments.** This work was supported by the KIP Pilot Project (kzcx2-yw-123) of the Chinese Academy of Sciences (CAS), National Important Basic Research Project (2006CB806306, 2011CB811405), and National Science Foundation of China (41004070, 40725014, 40636032, 40974090), Knowledge Innovation Program of the CAS, and China Postdoctoral Science Foundation. We are grateful to the ROCSAT team for access to the data at the Web site http://csrsddc.csrsr.ncu.edu.tw.

[23] Robert Lysak thanks Jan Lastovicka and another reviewer for their assistance in evaluating this paper.

References

Aruliah, A. L., A. D. Farmer, T. J. Fuller-Rowell, M. N. Wild, M. Hapgood, and D. Rees (1996), An equinoctial asymmetry in the high-latitude thermosphere and ionosphere, *J. Geophys. Res.*, *101*(A7), 15713–15722, doi:10.1029/95JA01102.

Bailey, G. J., Y. Z. Su, and K.-I. Oyama (2000), Yearly variations in the low-latitude topside ionosphere, *Ann. Geophys.*, *18*, 789–798.

Balan, N., Y. Otsuka, S. Fukao, and G. J. Bailey (1998), Equinoctial asymmetries in the ionosphere and thermosphere observed by the MU radar, *J. Geophys. Res.*, *103*(A5), 9481–9486, doi:10.1029/97JA03137.

Balan, N., S. Kawamura, T. Nakamura, M. Yamamoto, S. Fukao, W. L. Oliver, M. E. Hagan, A. D. Aylward, and H. Alleyne (2006), Simultaneous mesosphere–lower thermosphere and thermospheric *F*-region observations using middle and upper atmosphere radar, *J. Geophys. Res.*, *111*, A10S17, doi:10.1029/2005JA011487.

Crain, D. J., R. A. Heelis, and G. J. Bailey (1993), Effects of electrical coupling on equatorial ionospheric plasma motions: When is the *F* region a dominant driver in the low-latitude dynamo, *J. Geophys. Res.*, *98*(A4), 6033– 6037, doi:10.1029/92JA02195.

Dunkerton, T. (1982), Theory of the mesopause semiannual oscillation, *J. Atmos. Sci.*, *39*, 2681–2690.

England, S. L., S. Maus, T. J. Immel, and S. B. Mende (2006), Longitudinal variation of the E-region electric fields caused by atmospheric tides, *Geophys. Res. Lett.*, *33*, L21105, doi:10.1029/2006GL027465.

Essex, E. A. (1977), Equinoctial variations in the total electron content of the ionosphere at northern and southern hemisphere stations, *J. Atmos. Terr. Phys.*, *39*, 645–650.

Fejer, B. G., E. R. de Paula, S. A. Gonzalez, and R. F. Woodman (1991), Average vertical and zonal *F* region plasma drifts over Jicamarca, *J. Geophys. Res.*, *96*(A8), 13901–13906, doi:10.1029/91JA01171.

Fejer, B. G., J. W. Jensen, and S.-Y. Su (2008), Quiet time equatorial F region vertical plasma drift model derived from ROCSAT-1 observations, *J. Geophys. Res.*, *113*, A05304, doi:10.1029/2007JA012801.

Forbes, J. M. (1995), Tidal and planetary waves, in *The Upper Mesosphere and Lower Thermosphere: A Review of Experiment and Theory*, *Geophys. Monogr. Ser.*, vol. 87. edited by R. M. Johnson and T. L. Killeen, pp. 67–87, Am. Geophys. Union, Washington, D.C.

Forbes, J. M., R. G. Roble, and C. Fesen (1993), Acceleration, heating, and compositional mixing of the thermosphere due to upward propagating tides, *J. Geophys. Res.*, *98*(A1), 311–321, doi:10.1029/92JA00442.

Garcia, R., T. Dunkerton, R. Lieberman, and R. Vincent (1997), Climatology of the semiannual oscillation of the tropical middle atmosphere, *J. Geophys. Res.*, *102*(D22), 26019–26032, doi:10.1029/97JD00207.

Hartman, W. A., and R. A. Heelis (2007), Longitudinal variations in the equatorial vertical drift in the topside ionosphere, *J. Geophys. Res.*, *112*, A03305, doi:10.1029/2006JA011773.

Häusler, K., and H. Lühr (2009), Nonmigrating tidal signals in the upper thermospheric zonal wind at equatorial latitudes as observed by CHAMP, *Ann. Geophys.*, *27*(7), 2643–2652.

Heelis, R. A. (2004), Electrodynamics in the low and middle latitude ionosphere: A tutorial, *J. Atmos. Sol. Terr. Phys.*, *66*(10), 825–838.

Kawamura, S., N. Balan, Y. Otsuka, and S. Fukao (2002), Annual and semiannual variations of the midlatitude ionosphere under low solar activity, *J. Geophys. Res.*, *107*(A8), 1166, doi:10.1029/2001JA000267.

Kil, H., S.-J. Oh, M. C. Kelley, L. J. Paxton, S. L. England, E. Talaat, K.-W. Min, and S.-Y. Su (2007), Longitudinal structure of the vertical $\mathbf{E} \times \mathbf{B}$ drift and ion density seen from ROCSAT-1, *Geophys. Res. Lett.*, *34*, L14110, doi:10.1029/2007GL030018.

Kil, H., S.-J. Oh, L. J. Paxton, and T.-W. Fang (2009), High-resolution vertical $\mathbf{E} \times \mathbf{B}$ drift model derived from ROCSAT-1 data, *J. Geophys. Res.*, *114*, A10314, doi:10.1029/2009JA014324.

Liu, H., H. Lühr, and S. Watanabe (2007), Climatology of the equatorial thermospheric mass density anomaly, *J. Geophys. Res.*, *112*, A05305, doi:10.1029/2006JA012199.

Liu, L., X. Luan, W. Wan, J. Lei, and B. Ning (2003), Seasonal behavior of equivalent winds over Wuhan derived from ionospheric data in 2000–2001, *Adv. Space Res.*, *32*(9), 1765–1770.

Liu, L., B. Zhao, W. Wan, S. Venkartraman, M.-L. Zhang, and X. Yue (2007), Yearly variations of global plasma densities in the topside ionosphere at middle and low latitudes, *J. Geophys. Res.*, *112*, A07303, doi:10.1029/2007JA012283.

Liu, L., B. Zhao, W. Wan, B. Ning, M.-L. Zhang, and M. He (2009), Seasonal variations of the ionospheric electron densities retrieved from Constellation Observing System for Meteorology, Ionosphere, and Climate mission radio occultation measurements, *J. Geophys. Res.*, *114*, A02302, doi:10.1029/2008JA013819.

Liu, L., M. He, X. Yue, B. Ning, and W. Wan (2010), Ionosphere around equinoxes during low solar activity, *J. Geophys. Res.*, *115*, A09307, doi:10.1029/2010JA015318.

Ma, R., J. Xu, and H. Liao (2003), The features and a possible mechanism of semiannual variation in the peak electron density of the low latitude F2 layer, *J. Atmos. Solar-Terr. Phys.*, *65*, 47–57.

Mayr, H. G., and K. K. Mahajan (1971), Seasonal variation in the F_2 region, *J. Geophys. Res.*, *76*(4), 1017-1027, doi:10.1029/JA076i004p01017.

Mendillo, M., C. Huang, X. Pi, H. Rishbeth, and R. Meier (2005), The global ionospheric asymmetry in total electron content, *J. Atmos. Solar-Terr. Phys.*, *67*, 1377–1387.

Millward, G. H., I. C. F. Müller-Wodarg, A. D. Aylward, T. J. Fuller-Rowell, A.D. Richmond, and R. J. Moffett (2001), An investigation into the influence of tidal forcing on *F*-region equatorial vertical ion drift using a global ionosphere thermosphere model with coupled electrodynamics, *J. Geophys. Res.*, *106*(A11), 24,733–24,744, doi:10.1029/2000JA000342.

Mukhtarov, P., D. Pancheva, and B. Andonov (2009), Global structure and seasonal and interannual variability of the migrating diurnal tide seen in the SABER/TIMED temperatures between 20 and 120 km, *J. Geophys. Res.*, *114*, A02309, doi:10.1029/2008JA013759.

Oberheide, J., and J. M. Forbes (2008), Tidal propagation of deep tropical cloud signatures into the thermosphere, *Geophys. Res. Lett.*, *35*, L04816, doi:10.1029/2007GL032397.

Pancheva, D., and P. Mukhtarov (2010), Strong evidence for the tidal control on the longitudinal structure of the ionospheric *F* region, *Geophys. Res. Lett.*, *37*, L14105, doi:10.1029/2010GL044039.

Ren, Z., W. Wan, L. Liu, B. Zhao, Y. Wei, X. Yue, and R. A. Heelis (2008), Longitudinal variations of electron temperature and total ion density in the sunset equatorial topside ionosphere, *Geophys. Res. Lett.*, *35*, L05108, doi:10.1029/2007GL032998.

Ren, Z., W. Wan, L. Liu, and J. Xiong (2009a), Intra-annual variation of wave number 4 structure of vertical $\mathbf{E} \times \mathbf{B}$ drifts in the equatorial ionosphere seen from ROCSAT-1, *J. Geophys. Res.*, *114*, A05308, doi:10.1029/2009JA014060.

Ren, Z., W. Wan, L. Liu, R. A. Heelis, B. Zhao, Y. Wei, and X. Yue (2009b), Influences of geomagnetic fields on longitudinal variations of vertical plasma drifts in the presunset equatorial topside ionosphere, *J. Geophys. Res.*, *114*, A03305, doi:10.1029/2008JA013675.

Ren, Z., W. Wan, J. Xiong, and L. Liu (2010), Simulated wave number 4 structure in equatorial *F*-region vertical plasma drifts, *J. Geophys. Res.*, *115*, A05301, doi:10.1029/2009JA014746.

Rishbeth, H. (2004), Questions of the equatorial F2-layer and thermosphere, *J. Atmos. Solar-Terr. Phys.*, *66*, 1669-1674.

Rishbeth, H., I. C. F. Müller-Wodarg, L. Zou, T. J. Fuller-Rowell, G. H. Millward, R. J. Moffett, D. W. Idenden, and A. D. Aylward (2000), Annual and semiannual variations in the ionospheric F2-layer: II. Physical discussion, *Ann. Geophys.*, *18*, 945-956.

Titheridge, J. E. (1973), The electron content of the southern mid-latitude ionosphere, 1965–1971, *J. Atmos. Terr. Phys.*, *35*, 981–1001.

Titheridge, J. E. (1997), Model results for the ionospheric E region: Solar and seasonal changes, *Ann. Geophys.*, *15*(1), 63–78.

Titheridge, J. E., and M. J. Buonsanto (1983), Annual variations in the electron content and height of the F layer in the Northern and Southern Hemispheres, related to neutral composition, *J. Atmos. Terr. Phys.*, *45*, 683–696.

Unnikrishnan, K., R. B. Nair, and C. Venugopal (2002), Harmonic analysis and an empirical model for tEC over Palehua, *J. Atmos. Solar-Terr. Phys.*, *64*, 1833–1840.

Wan, W., L. Liu, X. Pi, M.-L. Zhang, B. Ning, J. Xiong, and F. Ding (2008), Wave number-four patterns of the total electron content over the low latitude ionosphere, *Geophys. Res. Lett.*, *35*, L12104, doi:10.1029/2008GL033755.

Xu, J., A. K. Smith, H.-L. Liu, W. Yuan, Q. Wu, G. Jiang, M. G. Mlynczak, J. M. Russell III, and S. J. Franke (2009), Seasonal and quasi-biennial variations in the migrating diurnal tide observed by Thermosphere, Ionosphere, Mesosphere, Energetics and Dynamics (TIMED), *J. Geophys. Res.*, *114*, D13107, doi:10.1029/2008JD011298.

Yue, X., W. Wan, L. Liu, H. Le, Y. Chen, and T. Yu (2008), Development of a middle and low latitude theoretical ionospheric model and an observation system data assimilation experiment, *Chin. Sci. Bull.*, *53*(1), 94–101.

Zhang, S.-R., J. M. Holt, A. M. Zalucha, and C. Amory-Mazaudier (2004), Midlatitude ionospheric plasma temperature climatology and empirical model based on Saint Santin incoherent scatter radar data from 1966 to 1987, *J. Geophys. Res.*, *109*, A11311, doi:10.1029/2004JA010709.

Zhang, S.-R., J. M. Holt, A. P. van Eyken, M. McCready, C. Amory–Mazaudier, S. Fukao, and M. Sulzer (2005), Ionospheric local model and

climatology from long–term databases of multiple incoherent scatter radars, *Geophys. Res. Lett.*, *32*, L20102, doi:10.1029/2005GL023603.

Zhang, S.-R., and J. M. Holt (2007), Ionospheric climatology and variability from long–term and multiple incoherent scatter radar observations: Climatology in eastern American sector, *J. Geophys. Res.*, *112*, A06328, doi:10.1029/2006JA012206.

Zhao, B., W. Wan, L. Liu, T. Mao, Z. Ren, M. Wang, and A. B. Christensen (2007), Features of annual and semiannual variations derived from the global ionospheric maps of total electron content, *Ann. Geophys.*, *25*, 2513–2527.

Y. Chen, H. Le, L. Liu, Z. Ren, and W. Wan, Beijing National Observatory of Space Environment, Institute of Geology and Geophysics, Chinese Academy of Sciences, Beijing 100012, China. (wanw@mail.iggcas.ac.cn)